Rula Alrawashdeh

Mutah University , Jordan

doi:10.15199/48.2020.07.24

Patch antenna based on spiral split rings for bone implants

Abstract. *In this paper, a patch antenna based on spiral split rings is proposed for bone implants in the 401-406 MHz Medical Device Radiocommunications Service (MedRadio) and 433-434 MHz Industrial, Scientific and Medical (ISM) bands. The antenna is small of only 7 mm in radius and 3 mm in thickness. It has obtained maximum gains of -36.8 and -35.6 dBi at 403 and 433 MHz, respectively in a simplified multilayer leg model. The antenna has a robust performance that is verified in simplified leg models of an adult and a child. It can communicate over a distance of longer than 12 m in an indoor environment. The antenna proposed in this paper is probably the smallest reported bone implantable antenna that works for the 401-406 MedRadio and 433-434 MHz ISM bands. The effect of the structure parameters on the antenna performance is investigated which provides guidelines for other designs inspired by such a structure.*

Streszczenie. *W artykule zaprezentowano projekt anteny bazującej na spralnych pierścieniach. Antenę zaprojektowaniu do umieszczenia w implantach kości i możliwości zastosowania w zakresie 401-406 MHz (zakres do zastosowań medycznych) lub 433-434 MHz. Średnica anteny nie przekracza 7 mm a grubość 3 mm.* ***Projekt anteny bazującej na spiralnych pierścieniach do zastosowań medycznych – implantów kości..***

Keywords: Bone implants, ISM, MedRadio, Spiral split ring
Słowa kluczowe: implanty kości, antena

Introduction

Implantable antennas are used to transfer data from inside human body tissues such as muscles and bones to an external receiver at which data are processed by a physician or doctor. This enables wide range of beneficial applications such as wireless post surgery checkups and glucose monitoring [1-3]. The signals are susceptible to attenuation losses in the human body tissue layers and reflection at the boundaries between them. These losses increase when the signals pass through more tissues such as the case of bone implants in comparison with that of muscle implants [4]. The attenuation losses are decreased if specific types of antennas that enclose larger near magnetic field than near electric field are used. This is because the human body is non-magnetic and does not present magnetic losses [5]. The implantable antenna should be small in size to fit inside the implant and resonate in the (401-406 MHz) Medical Device Radiocommunication Service (MedRadio) band at the same time [6-7]. The Specific Absorption Rate (SAR) limitations (1-g avg SAR<1.6 W/kg) [8] and (10-g avg SAR< 2 W/kg) [9]) should be also satisfied. It is also preferred to work for the 433-434.8 MHz ISM band to support the functionality of wireless power transfer [10]. Patch antennas have many attractive features to satisfy these requirements. They can be designed with different patch shapes which can be optimized to obtain miniaturization and to enclose a relatively large near magnetic field such as spirals and split rings [11-13]. Also, as patch antennas have ground in their structure, they usually obtain small SAR rates [14]. Different designs of patch antennas for implantable applications were proposed in literature [15-16]. Planar Inverted-F antenna (PIFA) was mainly designed [17-19]. However, it usually has a narrow bandwidth which does not guarantee a robust performance in the real human body [5, 20]. The bandwidth is expected to become narrower in tissues such as bones than that of muscle [4]. This is because bones have smaller relative permittivity than that of muscle which requires further miniaturization. Structures based on spirals usually obtain a relatively wide bandwidth [21]. Some spiral patch antennas were proposed for muscle implants such as in [5, 22]. However, most of these antennas were relatively large in size and they are expected to become larger in bone. Hence, structures that provide further miniaturization are needed for the design of small antennas in bone tissues [4]. Spiral resonators were shown to provide stronger miniaturization than that for typical spirals [23]. This is because they exploit splits in their structure. Structures based on split rings and complementary split rings can increase the implantable antenna radiation efficiency and gain [24]. Therefore, a structure based on them is exploited for the design in this paper. The attractive features of the spiral combined with that for split rings could provide many advantages for implantable applications especially for bone implantable antennas which are required to obtain comparable radiation efficiency and gain values to muscle implantable antennas despite of the extra losses introduced from propagation in bones and at the muscle-bone boundary. Few antennas were proposed for bone implants in literature. In [25], a slotted waveguide antenna was provided to work at 20 GHz. However, that design exploited the entire wall of a large implant that was 70 mm in length. Moreover, the attenuation losses were large at this frequency than that at around 403 MHz. In [26], a square loop was proposed for an implantable RFID in the tibia bone at 870-960 MHz. A spiral antenna was proposed for bone implants at 2.45 GHz in [27]. However, that antenna was narrow in bandwidth (BW≈ 1%). All of these antennas work for bands other than the MedRadio band that is mainly allocated for implantable applications. Meandered loop antennas were proposed in [28] for total knee replacement implants in the 401-406 MHz MedRadio band and in [4] for general bone implants in the 401-406 MHz MedRadio and 433-434.8 MHz ISM bands. However, they exploited the entire outer wall of a large cylindrical bone implant that was 40 mm in length. All previous designs of bone implantable antennas were either proposed at frequency bands other than the 401-406 MHz MedRadio band or were designed for bone implants of specific shapes exploiting their entire structure. Therefore, small patch antennas are still needed for small bone implants that work for the 401-406 MHz MedRadio band. Hence, a patch antenna based on spiral split rings is aimed for the design in this paper. The appealing features of patch antennas combined with that for spiral split rings are exploited to optimize an implantable antenna for small bone implants. Up to the author's best knowledge this antenna is the smallest patch antenna proposed for bone implants in the 401-406 MHz MedRadio and 433-434.8 MHz ISM bands. The effective design parameters of the proposed structure are investigated which provides guidelines for other designs exploiting such a structure. This paper is organized as follows: In Section 2 the antenna design is proposed and its performance in a simplified multilayer body model is evaluated and

discussed. Then, the performance is validated in adult and child leg models in Section 3. The communication range supported by this antenna in an indoor environment is also calculated in this section. The related issues of biocompatibility and SAR are discussed in Section 4 and the paper is finally concluded in Section 5.

Design and performance

The structure of the proposed antenna is shown in Fig.1. The antenna is circular in shape and is composed of ground, substrate (ε_r= 3, h= 3 mm) and patch. It is composed of three spiral split rings. Its outer ring is 7 mm in radius. The antenna is fed by a coaxial cable which has a dielectric of ε_r = 3 and outer and inner radii of 0.5 and 0.3 mm, respectively. The final antenna parameters are summarized in Table 1.

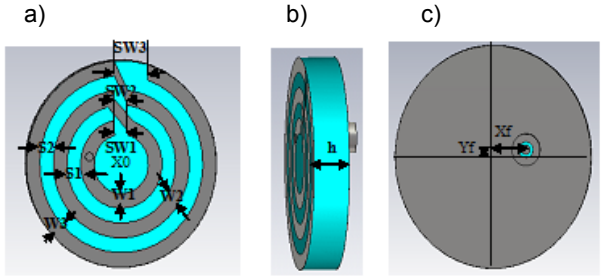

Fig.1. The proposed antenna: a) Front view, b) Side view, and c) Back view

Table 1. Optimized parameters of the proposed antenna

Horizontal distance between the ground and feed centers	*Xf*	2.35
Vertical distance between the ground and feed centers	*Yf*	0.5
Inner ring width	*W1*	1
Mid ring width	*W2*	1
Outer ring width	*W3*	1
Spacing between the inner and mid rings	*S1*	1
Spacing between the mid and outer rings	*S2*	1
Inner ring split width	*SW1*	1
Mid ring split width	*SW2*	1
Outer ring split width	*SW3*	1.95
Substrate thickness	*h*	3

The antenna parameters are optimized to obtain resonance in the 401-406 MHz MedRadio and 433-434 MHz ISM bands in a simplified multilayer body model. This model is shown in Fig. 2. It is cylindrical in shape which resembles the shape of a human leg and has four tissue layers: cortical bone (ε_r= 13.1 and σ = 0.09 S/m), muscle (ε_r = 57.1 and σ= 0.79 S/m), fat (ε_r = 5.6 and σ = 0.04 S/m) and skin (ε_r =46.7 and σ = 0.69 S/m). The dielectric properties of the human body tissues are frequency dependent and the values mentioned above are obtained from [29] for the human body tissues at 403 MHz. The thicknesses of the bone, muscle, fat and skin layers are 70, 30, 2, and 4 mm, respectively. The antenna is first designed in a short body model of 40 mm length only. This is to optimize the antenna parameters for resonance in the desired bands within short simulation time while obtaining accurate results at the same time [30].

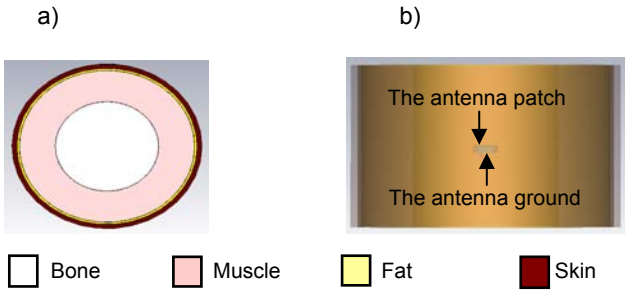

Fig.2. The body model of simulations: a) Top view, b) Side view

The antenna has obtained a -10 dB bandwidth of 68.3 MHz ranging from 370.5 MHz to 438.8 MHz (*BW*: 16.9%) which covers both of the 401-406 MHz MedRadio and 433-434.8 MHz ISM bands as shown in Fig. 3.

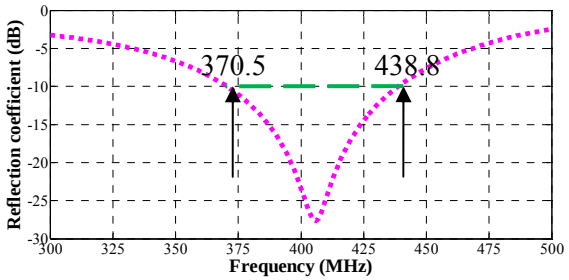

Fig.3. The reflection coefficient S_{11}(dB) of the proposed antenna

Increasing the split width of the outer ring (*SW3*) from 1 to 1.95 mm that works as the spacing between the plates of a parallel plate capacitor (d (m)) decreases the capacitance (C (F)) (1) [31]:

$$C = \frac{\varepsilon A}{d} \tag{1}$$

where A (m^2) is the plate area and ε (F/m) is the dielectric permittivity.

The reduction in the capacitance shifts the resonance up by 10.2 MHz. The upper band limit is thus shifted up from 428.6 to 438.8 MHz which enables the coverage of the 433-434.8 MHz ISM as shown in Fig.4.

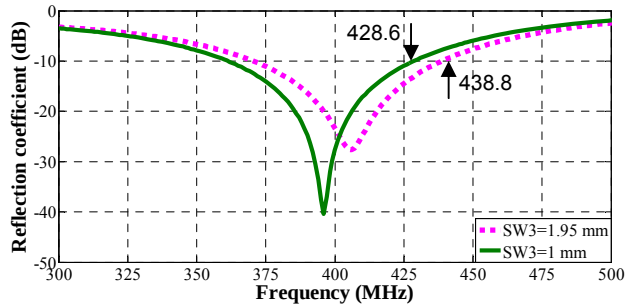

Fig.4. The reflection coefficient S_{11} (dB) of the proposed antenna for *SW3*= 1 and 1.95 mm

Another parameter that affects the resonance is the spacing between the rings (*S1*, *S2*). When it decreases the capacitance (C (F)) increases which shifts the resonant frequency down [32]. However, *S1* and *S2* are decreased by increasing the ring width (W). When the ring width (W) increases, the inductance (L (H)) decreases (2) [33]. The reduction of the inductance shifts the resonant frequency up [32].

$$L = \frac{\mu_0 l}{2\pi}\left(\ln\frac{4l}{W} - 2.45\right) \tag{2}$$

where μ_0(H/m) is the free space permeability, W (m) is the ring width which could be $W1$ or $W2$ or $W3$ for this case and l (m) is the circumference of the ring.
The effect of L and C on the resonant frequency (f_r (Hz)) is indicated in (3) [32]:

$$f_r = \frac{1}{2\pi\sqrt{LC}} \tag{3}$$

The following combinations of the ring width are investigated: ($W1$= 0.6, $W2$= 0.5 and $W3$= 1 mm), ($W1$= 1, $W2$= 1 and $W3$= 1 mm) and ($W1$= 2, $W2$= 1.5 and $W3$= 1 mm). The reflection coefficient S_{11} (dB) for these combinations is shown in Fig. 5.

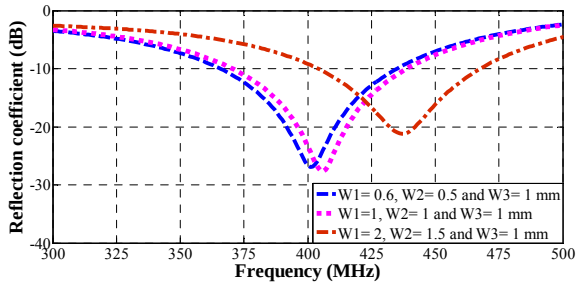

Fig.5. The reflection coefficient S_{11} (dB) for different combinations of ring widths

It can be seen from the figure that the resonant frequency is shifted up when the width of the inner and mid ring increase. It is shifted up by 5 MHz when the width of the inner and mid rings is increased by 0.4 and 0.5 mm, respectively and by 31 MHz when the width of the inner and mid rings is increased by 1 and 0.5 mm, respectively. This is because the total inductance is decreased for this case. Although the capacitance is increased, the resonant frequency is shifted up. This is because $W2$ becomes wider by decreasing $S2$ while $W1$ becomes wider towards $X0$ without changing $S1$ and hence both of $W1$ and $W2$ contribute to the reduction of L while only $S2$ contributes to the increase in the capacitance.

a)

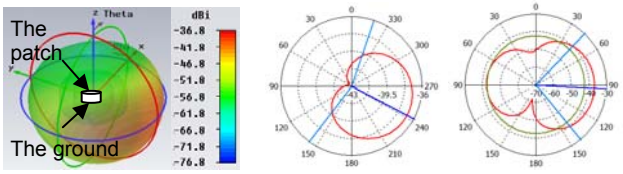

b)

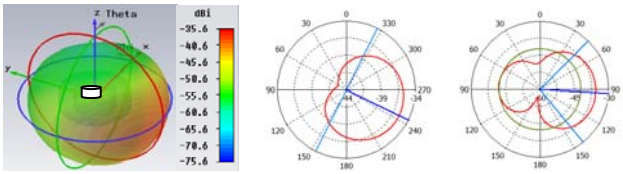

Fig.6. The 3D, xy and xz-radiation patterns of the proposed antenna at: a) 403 MHz, b) 433 MHz

The antenna has obtained a gain/radiation efficiency of -36.8 dBi/0.01% and -35.6 dBi/0.015% at 403 MHz and 433 MHz, respectively. The radiation efficiency and gain are larger at 433 MHz than that at 403 MHz as the antenna has a larger electrical size at this frequency. The antenna has obtained the maximum radiation in a desired direction away from the human body (at around 242^o in the xy-plane) as shown in Fig. 6. The same shape and direction of the maximum radiation are almost obtained at 403 and 433 MHz.

The surface current distribution is shown in Fig. 7. The figure shows that the strongest current is concentrated in close proximity to the feed. A strong current is also distributed on the rings themselves. As expected a weak surface current is noticed on the ground which does not contribute in the antenna main radiation. Stronger surface currents (such as that enclosed by dashed circles) are noticed on the radiating rings at 433 MHz than that at 403 MHz as the radiator is electrically larger at this frequency than that at 403 MHz.

a)

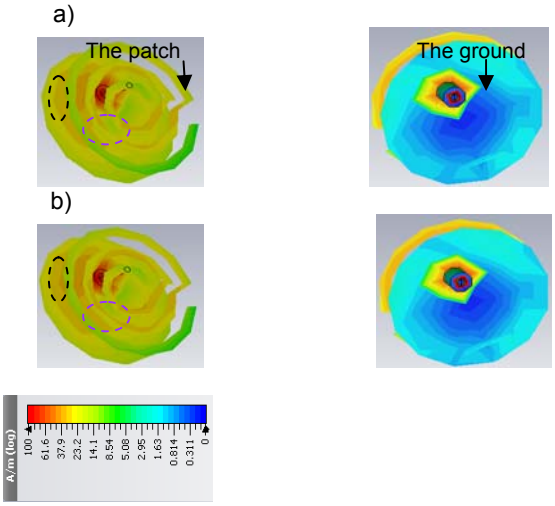

Fig.7. The surface current at: a) 403 MHz, b) 433 MHz

.

Validation in adult and child leg models

The resonant frequency is almost unaffected by the size of the body model. However, the radiation efficiency and gain become smaller in larger body models. The antenna performance is evaluated in two other models of larger size that resemble adult and child legs. These models are of the same shape and structure of the small body of optimization. The layer thicknesses and length of each model is summarized in Table 2. The lengths of these models are selected based on data available in [34-35].

Table 2. The dimensions of the simplified adult and child leg models

Model	Thickness (mm)				Length (mm)
	Bone	Muscle	Fat	Skin	
Adult	70	30	4	2	350
Child	40	20	2	2	280

The same resonant frequency and -10 dB bandwidth are obtained in all of the models. However, as expected smaller values of radiation efficiencies and gain than that in the smaller model of optimization are obtained. They are the smallest in the adult leg model as it has the largest size amongst all of these models. The results of the radiation efficiency and gain in these models are provided in Table 3. The main radiation pattern characteristics of the small model of optimization are maintained for the adult and leg models. The small values of the radiation efficiency and gain are expected in a lossy environment such as the human body. However, they satisfy the requirements of reliable communication over some distances which can be determined from link budget calculations. The following link budget is considered (4-5) [24]:

$$P_{rx} = P_{tx} + G_{tx} + G_{rx} - L_p \tag{4}$$

where P_{tx} and P_{rx} (dBm) are the transmitter and receiver antenna power, respectively, G_{tx} and G_{rx} (dBi) are the

transmitter and receiver antenna gain, respectively, L_p(dB) is the path propagation loss which can be obtained using (5) [24]:

$$L_p = 10n\log(\frac{r}{r_0}) + 10\log(\frac{4\pi d_0}{\lambda_0})^2 + S \quad (5)$$

where r (m) is the distance between the transmitter and receiver, r_0 (m) is a reference distance which is assumed to be 1 m, n is the path loss exponent, λ_0 (m) is the free space wavelength and S is the random scatter around the mean which is assumed to be zero.

Other losses such as the polarization and impedance mismatching losses are assumed to be zero for the well aligned and matched antennas of the transmitter and receiver. P_{tx} and P_{rx} are assumed to be 0 and -99 dBm, respectively [24]. G_{rx} is assumed to be 2.15 dBi as that for a standard dipole [24, 36]. The communication range r (m) is calculated for the three values of G_{tx}. Results of the possible communication ranges for the three G_{tx} values at 403 and 433 MHz are provided in Table 3.

Table 3. The total radiation efficiency, realized gain and possible communication range r (m) of the proposed antenna

The body model	Radiation efficiency (%)		G_{tx} (dBi) /r (m)	
	403 MHz	433 MHz	403 MHz	433 MHz
The short model of optimization	0.01	0.015	-36.8/21.2	-35.6/22.2
Adult leg	0.0073	0.0083	-38.8/18.2	-38.1/18.3
Child leg	0.009	0.013	-37.1/20.7	-36/21.5

Longer communication ranges are obtained at 433 MHz than that at 403 MHz. This is because the gain is larger at this frequency than that at 403 MHz. The shortest communication range is obtained for the case of the adult leg model as it has the smallest gain amongst all of these models. These communication ranges are long enough to place a receiver or transmitter at a far distance away from the human body which provides conformity to the patient. Extra losses are possible in the real human body which is not uniform in structure [24]. Thus, calculations are also conducted with an extra loss margin of 5 dB for the case of the adult model. The antenna can communicate over a distance of 12.4 and 12.47 m at 403 and 433 MHz, respectively in an indoor environment such as hospital rooms which are still far enough to provide conformity to the patient.

Biocompatibility and Specific Absorption Rate

The issues of biocompatibility and SAR are discussed in this section.

The proposed antenna is supposed to work inside a cylindrical implant of the biocompatible Polyethylene material (ε_r= 2.26, $\tan\delta$ = 0.0002 [28]). Matching can be still obtained for an implant of up to 0.2 mm in thickness and 5 mm in length. The radiation efficiency and gain are increased by around 5% and 0.3 dBi, respectively for this case. This is because the implant reduces the electric near field coupling with the surrounding human body tissues.

The specific absorption rate increases with the tissue conductivity and near electric field intensity while it decreases with the mass density (6) [37]:

$$SAR = \frac{\sigma|E|^2}{2\rho} \quad (6)$$

where σ (S/m) is the tissue conductivity, |E| (V/m) is the near electric field intensity and ρ (kg/m^3) is the tissue mass density.

The maximum 1-g avg rms SAR is computed for an input power of 1 W. The results are summarized in Table 4. The maximum input power is larger than 0 dBm that is usually provided to implantable devices. In accordance with the results in [24], the SAR decreases with frequency.

Table 4. The maximum 1-g avg rms SAR and allowed input power of the proposed antenna

The body model	Frequency (MHz)	1-g rms SAR	$P_{in,\ max}$ (mW/dBm)
The short model of optimization	403	147.1	5.4/7.3
	433	142.2	5.63/7.5
Adult leg	403	161.86	4.94/6.94
	433	154.4	5.18/7.14
Child leg	403	158.6	5.04/7.02
	433	146.7	5.45/7.36

A comparison of the main characteristics between the antenna proposed in this work and other bone implantable antennas reported in literature is provided in Table 5.

Table 5. A comparison between the antenna proposed in this work and other implantable bone antennas proposed in literature

Reference	Type	Freq (MHz)	Dimensions (mm)	G_{tx}(dBi)	BW (%)	Application
[4]	Elliptical meandered loop, one layer	326-454	30×40	-27.6 at 403 MHz	32.8	Monitoring of implants in the leg
[25]	Slotted waveguide	≈20900-21100	10×70	7.7 at 21 GHz	<1	Bone healing and growth
[26]	Square loop	870-960	6×75×4	-------	9.8	Tracking and sensing of Limb prosthesis
[27]	Spiral patch	2440-2465	2.6×2.6×1.94	-36.2 at 2.4 GHz	1	Health monitoring
[28]	Meandered loop, 3 planar layers	≈390-418	30×40	-21 at 403 MHz	6.9	Total knee replacement
[38]	Elliptical loop	220-440	56×36	-22 at 403 MHz	66.7	Implantable body sensor network
[39]	A pair of monopoles	1000-4000	- The radiating monopoles: 5×25 and 5×40 Grounds: 60×40 and 60×56	-------	120	Bone fracture monitoring
This work	Spiral split ring patch	370.5-438.8	14×14×3	-36.8 at 403 MHz	16.9	Monitoring of implants in Tibia

Few bone implantable antennas were reported in literature. Most of these antennas such as in [4, 25, 26, 28, 38, 39] were larger in size than the antenna proposed in this work. Although the antenna in [27] has a smaller size, it works at around 2.45 GHz. Also, that antenna obtained a very narrow bandwidth (≈1%) which does not guarantee a robust performance in the real human body. Moreover, that antenna obtained almost the same gain value of the proposed antenna although it is electrically larger. Although the gain of antennas in [4, 25, 28, 39] is larger than that of the proposed antenna, they were much larger in size. When the implant and antenna are larger in size, the area surrounds the implant becomes smaller which results in smaller absorption losses and larger radiation efficiency and gain are thus obtained. Also, as the antenna size increases, the gain increases [36]. The much larger size of the antennas in [4, 38, 39] than that of the proposed antenna justifies the wider bandwidth they obtained. To summary, the antenna proposed in this paper is the smallest bone implantable antenna proposed in literature to work for both of the 401-406 MHz MedRadio and 433-434.8 MHz ISM Bands. Unlike most of the bone implantable antennas proposed in literature, the proposed antenna can be used with bone implants of different structures and shapes (not only cylindrical implants).

Conclusion

In this paper, a small patch antenna based on spiral split rings is proposed for bone implantable applications. It works for the 401-406 MHz MedRadio and 433-434.8 MHz ISM bands. The antenna is 7 mm in radius and is 3 mm in thickness. The antenna has obtained gains of -36.8 and -35.6 dBi at 403 and 433 MHz, respectively in a simplified multilayer leg model. The antenna has obtained a robust performance in simplified leg models of an adult and a child. It can communicate over a distance longer than 12 m considering the worst case of indoor propagation from inside the real human body. The antenna has relatively small SAR rates which allow an average maximum input power of 5.27 W. The parameters of the split rings exploited on the antenna patch are investigated and their effect on the antenna performance is studied and discussed. This could provide guidelines for other designs based on this structure. The antenna proposed in this paper has many attractive features such as the small size, simple structure, robust performance and good radiation efficiency and gain which support communication in the farfield and hence providing a comfortable monitoring of the patient. It also supports the functionality of wireless power transfer. All of these features make this antenna a good candidate for bone implantable applications.

Authors
Dr. Rula Alrawashdeh, Department of Electrical Engineering, Mutah University, Alkarak-Jordan. E-mail: rularsr18@gmail.com

REFERENCES

[1] Ahmed A., Ur-Rehman M. and Abbasi Q. H., Miniature Implantable Antenna Design for Blood Glucose Monitoring, *2018 International Applied Computational Electromagnetics Society Symposium (ACES)*, Denver, CO, 2018, 1-2.

[2] Lakshmi P. S., Swetha D. and Jyothirmai P. S., Non-Invasive Measurement of Stress Levels in Knee Implants, *International Journal of Applied Engineering Research*, 14 (2019), No. 1, 308-312.

[3] Aleef T. A. and Biswas A., Design and Measurement of a Flexible Implantable Stripline-Fed Slot Antenna for Biomedical Applications, *2016 3rd International Conference on Electrical Engineering and Information Communication Technology (ICEEICT)*, Dhaka, 2016, 1-5.

[4] Alrawashdeh R., Huang Y and Sajak A. A. B., A Flexible Loop Antenna for Biomedical Bone Implants, *The 8th European Conference on Antennas and Propagation (EuCAP 2014)*, The Hague, 2014, 861-864.

[5] Merli. F, Implantable Antennas for Biomedical Applications, Ph.D. dissertation, EPFL University, Lausanne, Switzerland, 2011.

[6] Electromagnetic compatibility and Radio Spectrum Matters (ERM); Short Range Devices (SRD); Ultra Low Power Active Medical Implants (ULP-AMI) and Peripherals (ULP-AMI-P) operating in the frequency range 402 MHz to 405 MHz; Part 1 and Part 2, European Telecommunications Standards Institute (ETSI) Std. EN 301 839-1/2 V1.3.1, 2007. [Online]. Available: www.etsi.org

[7] Electromagnetic compatibility and Radio Spectrum Matters (ERM); Short Range Devices (SRD); Ultra Low Power Active Medical Implants (ULP-AMI) and Peripherals (ULP-AMI-P) operating in the frequency range 401 MHz to 402 MHz and 405 MHz to 406 MHz; Part 1, European Telecommunications Standards Institute (ETSI) Std. EN 302 537-1 V1.3.1, 2007. [Online]. Available: www.etsi.org

[8] IEEE Standard for Safety Levels with Respect to Human Exposure to Radio Frequency Electromagnetic Fields, 3 kHz to 300 GHz, IEEE Standard C95.1-1999, 1999.

[9] IEEE Standard for Safety Levels with Respect to Human Exposure to Radio Frequency Electromagnetic Fields, 3 kHz to 300 GHz, IEEE Standard C95.1-2005, 2005.

[10] Nikita K. S., Handbook of Biomedical Telemetry, Hoboken, New Jersey: John Wiley & Sons, 2014.

[11] Loktongbam P., and Laishram R., Performance and Design Analysis of an Implantable Antenna for Biotelemetry, *International Journal of Scientific and Research Publications*, 7 (2017), No. 6, 105-114.

[12] Liu C., Guo Y-X. and Xiao S., A Review of Implantable Antennas for Wireless Biomedical Devices, *Forum for Electromagnetic Research Methods and Application Technologies (FERMAT),* 2015, 1-11.

[13] Usman M., Alsaif H., M. Chughtai M., Asif S., Design of Compact Ultra-Wideband Monopole Semi-Circular Patch Antenna for 5G wireless communication networks, *Przeglad Elektrotechniczny*, 2019, No. 4, 223-226.

[14] Miozzi C., Saggio G., Gruppioni E. and Marrocco G., Performance Comparison of Patch and Loop Antennas for the Wireless Power Transfer and Transcutaneous Telemetry in the 860–960 MHz Frequency Band, *2019 IEEE 16th International Conference on Wearable and Implantable Body Sensor Networks (BSN)*, Chicago, IL, USA, 2019, 1-4.

[15] Mokhtar M., *et al*., Implantable Patch Antenna for Body Communication, *2018 2nd International Conference on Telematics and Future Generation Networks (TAFGEN)*, Kuching, 2018, 77-80.

[16] Fan Y., Liu X., Li J. and Chang T., A Miniaturized Circularly-Polarized Antenna for In-Body Wireless Communications, *Micromachines*, 10 (2019), No. 70, pp.1-11.

[17] Mahalakshmi N., and Thenmozhi A., Design of Hexagon Shape Bow-Tie Patch Antenna for Implantable Bio-Medical Applications, *Alexandria Engineering Journal*, 56 (2017), No. 2, 235-239, 2017.

[18] P. Soontornpipit*,* Design of Implanted PIFA for Implantable Biotelemetry Locations: Chest and Abdomen*, Procedia Computer Sciece*, 86 *(2016),* 236-239.

[19] Djellid A., Pichon L., Koulouridis S., and Bouttout F., Miniaturization of a PIFA Antenna for Biomedical Applications Using Artificial Neural Networks, *Progress In Electromagnetics Research M*, 70 (2018), 1–10.

[20] Kiourti A., and Nikita K., Miniature Scalp-Implantable Antennas for Telemetry in the MICS and ISM Bands: Design, Safety Considerations and Link Budget Analysis, *IEEE Transactions on Antennas Propagation*, 60 (2012), No. 8, 3568-3575.

[21] Basir A., et al., A Dual-Band Implantable Antenna with Wide-Band Characteristics at MICS and ISM Bands, *Microwave and Optical Technology Letters*, 60 (2018), No. 12, 2944-2949.

[22] Mahalakshmi N., and Thenmozhi A., Design and Development of Dual-Spiral Antenna for Implantable Biomedical Application, *Biomedical Research*, 28 (2017), No. 12, 5237-5240.

[23] Duran-Sindreu M., Naqui J., Paredes F., Bonache J., and Marti F., Electrically Small Resonators for Planar Metamaterial, Microwave Circuit and Antenna Design: A Comparative Analysis, *Applied Sciences*, 2 (2012), No. 4, 375-395.
[24] Alrawashdeh R.S., Huang Y., Kod M., and Sajak A. A. B., A Broadband Flexible Implantable Loop Antenna with Complementary Split Ring Resonators, *IEEE Antennas and Wireless Propagation Letters*, 14 (2015), 1506-1509.
[25] Zakavi P., Karmakar N. C., and Griggs I., "Wireless Orthopedic Pin for Bone Healing and Growth: Antenna Development, *IEEE Transactions on Antennas and Propagation*, 58 (2010), No. 12, 4069-4074.
[26] Lodato R., and Marrocco G., Close Integration of a UHF-RFID Transponder Into a Limb Prosthesis for Tracking and Sensing, *IEEE Sensors Journal*, 16 (2016), No. 6, 1806-1813.
[27] Khokle R. P., Esselle K. P., Heimlich M., and Bokor D., Design of a Miniaturized Bone Implantable Antenna for a Wireless Implant Monitoring Device, *Loughborough Antennas and Propagation Conference (LAPC)*, Loughborough, 2017, 1-2.
[28] Alrawashdeh R., Huang Y. and Cao. P, A Flexible Loop Antenna for Total Knee Replacement Implants in the MedRadio Band, *2013 Loughborough Antennas and Propagation Conference (LAPC)*, Loughborough, 2013, 225-228.
[29] Andreuccetti D., Fossi R. and Petrucci C., Calculation of the dielectric properties of body tissues in the frequency range 10 Hz - 100 GHz, Institute for Applied Physics, Italian National Research Council, Florence (Italy), 1997. Accessed: Jan. 25, 2019. [Online]. Available: http://niremf.ifac.cnr.it/tissprop/
[30] Kiourti A., and Nikita K. S., Methodologies for Fast and Accurate Design of Implantable Antennas: Analysis and Comparison, *2013 7th European Conference on Antennas and Propagation (EuCAP)*, Gothenburg, 2013, 579-582.
[31] Hayt W., and Buck J., Engineering Electromagnetics, USA, New York: McGraw Hill, 2012.
[32] Ziolkowski R. W., and Erentok A., Metamaterial-Based Efficient Electrically Small Antennas, *IEEE Transactions on Antennas and Propagation*, 54 (2006), No. 7, 2113-2130.
[33] M. Sadiku, Elements of Electromagnetics, USA, Oxford: Oxford University Press, 2007.
[34] Papathanasopoulou V. A., Fotiadis D. I., and Massalas C. V., The Finite Element Method in the Quantification of the Loading Situation in the Human Femur, *The Fifth International Workshop on Mathematical Methods in Scattering Theory and Biomedical Technology*, 2002, 372-381.
[35] Ha J.H., *et al*., Distribution of Lengths of the Normal Femur and Tibia in Korean Children from Three to Sixteen Years of Age*, J Med Korean Sci*, 18 (2003), No. 5, 715-721.
[36] Huang Y., and Boyle K., Antennas from Theory to Practice, UK, Chichester: John Wiley & Sons Ltd, 2008
[37] Rodrigues A. O. et al., SAR Calculations in an Anatomically Realistic Model of the Head of Cellular Phone Users, The *Fourth International Conference on Computation in Electromagnetics*, Bournemouth, UK, 2002, 1-2.
[38] Alrawashdeh R., "Path Loss Estimation for Bone Implantable Applications," *Jordanian Journal of Computers and Infromation Technology (JJCIT)*, vol. 4, no. 2, pp. 94-101, Aug. 2018.
[39] Symeonidis *S. et al*., Bone Fracture Monitoring Using Implanted Antennas in the Radius Tibia and Phalange Heterogeneous Bone Phantoms, *Biomedical Physics and Engineering Express,* 4 (2018), No. 4, 1-19.